J. Microbiol. Biotechnol. (2002), **12**(2), 258–267

JOURNAL OF MICROBIOLOGY AND BIOTECHNOLOGY

© The Korean Society for Microbiology and Biotechnology

Flux Regulation Patterns and Energy Audit of *E. coli* B/r and K-12

LEE, JINWON[1]*, AKSHAY GOEL[2], MOHAMMAD M. ATAAI[2], AND MICHAEL M. DOMACH[3]

[1]*Department of Chemical Engineering, Kwangwoon University, Seoul 139-701, Korea*
[2]*Department of Chemical Engineering, University of Pittsburgh, Pittsburgh, PA 15219, U.S.A.*
[3]*Department of Chemical Engineering, Carnegie Mellon University, Pittsburgh, PA 15213, U.S.A.*

Received: October 19, 2001
Accepted: February 19, 2002

Abstract A flux determination methodology has been built which enables to develop constrained stoichiometric relationships and metabolic balances. The analysis differs from those developed for anaerobic growth conditions in that cell mass formation is a significant sink for carbon. When combined with experimental measurements, a determined system of equations results yielded tricarboxylic acid (TCA) cycle and glycolytic fluxes. The methodology was implemented to determine the fluxes of *E. coli* B/r and K12, and it was found that as the growth rate in a glucose minimal medium increased, the cells became increasing glycolytic and the TCA fluxes either leveled off or declined. The pattern identified for the TCA fluxes corresponded to α-ketoglutarate dehydrogenase's induction-repression pattern, thereby suggesting that the induction-repression of the enzyme could result in significant flux changes. When the minimum flux solution was contrasted to the glycolytic and TCA fluxes determined, two observations were made. First, the minimum flux could provide the cell's biosynthetic ATP requirements. Second, at a high growth rate in a glucose medium, the excess glycolytic flux exceeded that of the TCA cycle, which appeared to more closely match the biosynthetic needs.

Key words: Metabolic flux analysis, yield analysis, *E. coli*, TCA cycle, glycolytic pathway

Bacteria have been successfully employed for recombinant protein and biochemical production for years. However, the numerous and elaborated control systems utilized by bacteria have made production systems difficult to optimization through either directed mutation or medium formulation. Consequently, optimization remains largely a trial and error process, and many processes may not be fully optimized. Thus, significant benefits can accrue from improving the understanding of what metabolic control strategies are utilized, and how they are implemented. Investigation of the regulatory features of the pathways that provide raw materials and energy necessary for growth and product synthesis has been recognized to be an important starting point. Consequently, numerous strategies have been pursued which have yielded useful information and potential insights.

At the induction-repression level, much work has been performed on mapping the induction/repression trends of the glycolytic, pentose phosphate pathway, and TCA cycle enzymes [1, 4, 6, 8] in *E. coli*. These efforts have been aimed to identify which metabolic reactions are active under a given set of growth conditions, and where possible flux control points may reside [31]. However, because network flux control tends to be shared by all the enzymes in a pathway [11], translating changes in the amount of a particular enzyme into an impact on the network flux can be tenuous.

There have also been many studies on the kinetics of isolated enzymes. Such studies have elucidated reaction mechanisms and identified rate modulators. These results have, in turn, allowed for control mechanisms to be postulated, and maps with feedback loops developed. However, due to the absence of *in vivo* flux data, many mechanisms remain untested.

To bridge the gap between intact cell behavior and measurements of component properties, flux analysis frameworks have been used in conjunction with experimental data to deduce intracelluar metabolic fluxes. Although such approaches are not without limitations [17, 28], useful results have been obtained. For example, Holms [9] performed network calculations to map the metabolic fluxes in *E. coli* under a variety of growth conditions. The analysis assumed a constant cell yield and utilized known cellular composition profiles and metabolic reaction stoichiometries. Apart from predicting fluxes, some interesting ideas have also been generated on the efficiency associated with acetate production.

*Corresponding author
Phone: 82-2-940-5172; Fax: 82-2-909-0701;
E-mail: jwlee@gwu.ac.kr

More recently, metabolic measurements have been combined with network analyses to probe how the isocitrate branch point operates in *E. coli* [26]. The results revealed that the phosphorylation mechanism identified from *in vivo* experiments on isocitrate dehydrogenase indeed provides "ultrasensitive branch point control" *in vivo*.

On a similar theme, the current study mapped the fluxes of *E. coli* B/r and K12. The former has been used extensively in physiological studies; hence, acquiring additional information can contribute to tying together different facets of *E. coli* B physiology. In contrast, the K12 strain is better understood at the genetic level, and thus, is commonly employed as a host for recombinant protein production. Accordingly, obtaining metabolic flux information was envisioned to be useful for ultimately improving the understanding of the effects of recombinant protein expression on hosts.

This paper describes for the first time framework of analysis which parallels with Holms' [9], in that cellular composition data and biosynthetic stoichiometries were employed. However, many more direct measurements were also used in conjunction with a network analysis. Following the description of the approach, the results are presented for chemostat-cultivated *E. coli* B/r and K12. How the fluxes map to the reported activity profiles is then discussed, along with how the phosphoenolpyruvate and α-ketoglutarate branch points operate.

MATERIALS AND METHODS

Organisms and Culture Media

The wild-type *Escherichia coli* B/r was obtained from the American Type Culture Collection (ATCC number 12407). The cells were cultivated in a glucose minimal medium containing (in g/l): K_2HPO_4, 3; KH_2PO_4, 1.5; $(NH_4)_2SO_4$, 1.25; $MgSO_4$, 0.1; $FeSO_4$, 0.001; glucose, 1; NaCl, 0.01; $CaCl_2 \cdot 2H_2O$, 0.015; $MnCl_2 \cdot 4H_2O$, 0.015; $FeCl_3 \cdot 6H_2O$, 0.002; and antifoam C (purchased from SIGMA). The *E. coli* JM101 [32], which is a K12 strain and carries an F plasmid, was a generous gift from Dr. S. Khan (University of Pittsburgh, Pittsburgh, U.S.A.). The glucose minimal medium used to cultivate *E. coli* JM101 contained (in g/l): K_2HPO_4, 2.72; KH_2PO_4, 1.5; NH_4Cl, 1.0; Na_2SO_4, 0.284; $NaNO_3$, 0.17; KCl, 0.15; $MgCl_2 \cdot 6H_2O$, 0.049; $FeCl_3 \cdot 6H_2O$, 0.002; $MnCl_2 \cdot 4H_2O$, 0.158; $CaCl_2 \cdot 6H_2O$; and glucose, 1.0 [3]. Professor J. R. Guest (Sheffield University, Sheffield, U.K.) kindly provided a citrate synthase deficient mutant of *E. coli* W620 (F^- thi-1 pyrD36 gltA6 galK30 rpsL129 supE44 [22, 24]). The proline-supplemented minimal medium for *E. coli* W620 contained (in g/l): K_2HPO_4, 14; KH_2PO_4, 6; $MgSO_4$, 0.05; $(NH_4)_2SO_4$, 1.25; $FeSO_4$, 0.001; Na_3·citrate· $2H_2O$, 0.5; $CaCl_2 \cdot 2H_2O$, 0.015; thiamine, 0.005; uracil, 0.035; glucose, 2; and variable L-proline as noted for each experiment in the text [12]. The salts, glucose, and L-proline solutions were all steam-sterilized for 25 min at 121°C. The inoculum was prepared from a culture grown overnight in a shaker flask in the same medium.

Chemostat Experiments

The chemostat experiments were conducted in a 1-liter Applikon fermenter at various dilution rates and substrate concentrations. The cell concentrations were determined by measuring the optical density at 660 nm. The chemostat was deemed to have attained a steady-state when the CO_2 evolution rate stabilized after at least five retention times had passed. The temperature (fixed at 37°C) and pH in the fermenter were controlled by a Haake heating bath/ circulator and Cole-Parmer pH controller, respectively. The glucose concentration was measured off-line using an enzymatic assay kit purchased from the Sigma chemical company (Kit number 16).

The CO_2 evolution rate and O_2 consumption rate were measured on-line by a Dycor gas mass spectrometer; the data were accumulated by an IBM Personal Computer [2]. A standard gas mixture containing 98.012% N_2, 0.989% CO_2, and 0.999% O_2 was used to determine the correlation factors between the actual and measured values. For each experiment, the partial pressures of CO_2 and O_2 were normalized by the N_2 partial pressure for a comparison of each measurement. In practice, the correlation factors changed by less than 2%.

HPLC was used off-line to detect and quantify the organic byproducts (acetate, pyruvate, lactate, etc.) produced by the cells. A Bio-Rad HPLC column (model: Aminex HPX-87C) and UV detection at 210 nm were employed. The column was calibrated by injecting a known amount of each organic acid and determining the retention time and concentration-to-area relationship (peak area was calculated by computer software provided by Bio-Rad).

Batch Experiments

A fermenter (size 1-l) and proline-supplemented minimal medium were used for the batch experiments of *E. coli* W620. The agitation and air flow rate were kept constant throughout the experiment. The temperature of the culture medium (37°C) was controlled by a Haaks heating bath/ circulator. The optical cell density was measured at 550 nm.

METABOLIC FLUX AND YIELD ANALYSIS

Flux Analysis

A framework was developed to determine the carbon flux through glycolysis, TCA cycle, pentose phosphate pathway, and various biosynthetic pathways [13]. The fluxes accounted for are shown in Fig. 1. Each arrow indicates the net flux which occurs *in vivo*; in some

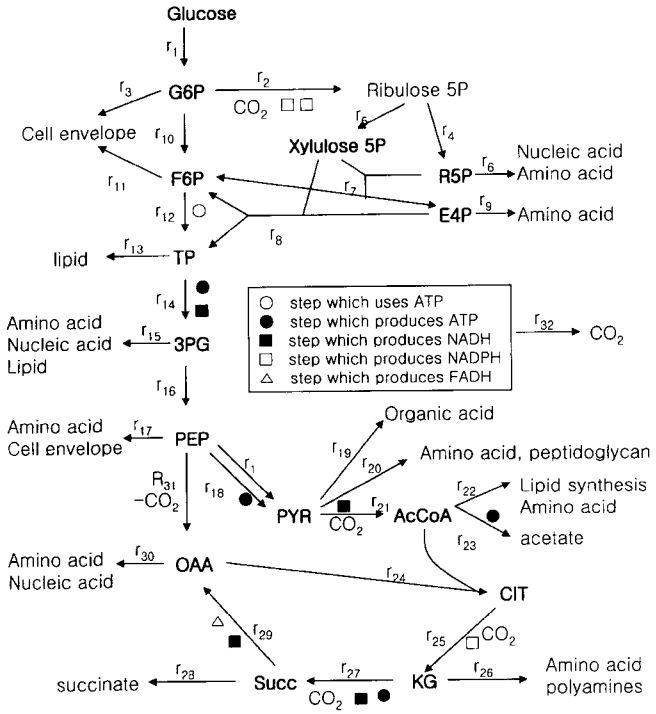

Fig. 1. Network analyzed to determine glycolytic, TCA cycle, and pentose phosphate pathway fluxes. Reactions producing ATP, NADH, NADPH, and FADH are shown (see symbol key).

instances, several reaction steps are skipped or simplified. To represent the dephosphorylation of phosphoenolpyruvate that is coupled to a glucose transport across the cell membrane [20], the dephosphorylation flux (r_1) is separated from the ATP-producing flux (r_{18}). Overall, 32 carbon compound fluxes are accounted for. These fluxes can be classified into three categories: (1) fluxes that connect the metabolite pools; (2) biosynthetic fluxes; and (3) fluxes for transporting carbon, organic acids, and CO_2 through the cell membrane.

For the 32 fluxes, four (r_1, r_{19}, r_{23}, r_{28}) can be measured, while the values of 11 (r_3, r_6, r_9, r_{11}, r_{13}, r_{15}, r_{17}, r_{20}, r_{22}, r_{26}, r_{30}) can be estimated from cell composition data and the stoichiometry of the biosynthetic reactions [10, 13, 16]. Moreover, the flux to the pentose phosphate pathway (r_2) and the TCA cycle flux (r_{25}) should provide the NADPH required for biosynthesis. The rate of CO_2 evolution (r_{32}) can be estimated from the pentose phosphate pathway and TCA cycle fluxes plus the amount of CO_2 produced as a byproduct of the biosynthetic reactions. The remaining 16 fluxes can be obtained from the material balances (See Appendix.).

Consistency Tests for Fluxes

The reliability of the means used to evaluate the fluxes can be assessed by determining if the overall balances and consistency tests are satisfied. The relevant equations are

$$r_{32,\,measured} = r_{32,\,calculated\ from\ equation\ (A1p)} \quad (1a)$$

$$6r_{1,\,measured} = (r_{19}+2r_{23}+4r_{28}+r_{32})_{measured} + 0.45D\ 1000/12 \quad (1b)$$

$$(\text{measured } O_2 \text{ consumption rate}) = (r_{14}+r_{21}+r_{27}+2r_{29})/2 + 3.578\ D/2 + (\text{any other NADH formation rate})/2 \quad (1c)$$

Equation (1a) compares the measured and predicted CO_2 evolution rates. The degree of the two equal rates indicates whether the correct fluxes have been assigned to the significant CO_2 evolving and consuming reactions (r_2, r_{21}, r_{25}, r_{27}, r_{31}, and evolution flux from biosynthesis). In the overall molar carbon balance (Eq. 1b), the measured rate of the total carbon consumption (left side) is contrasted to the carbon output rate (right side) in the form of organic acids (e.g. acetate, etc.), CO_2, and the biomass (assuming the biomass C content is 45% by weight). In Eq. (1b), β denotes the moles of carbon per mole of organics secreted from the pyruvate. This balance indicates whether the majority of significant carbon sinks and byproducts have been identified, accurately measured, and accounted for in the calculations. Equation (1c) contrasts the measured oxygen uptake rate (left side) and the predicted oxygen consumption rate (right side). The predicted rate is based on the fluxes that are coupled to NADH and $FADH_2$ formation, which includes the formation of NADH as a biosynthetic byproduct [10] and any metabolites whose formation is coupled to NADH reduction or oxidation (e.g. lactate and biosynthesis). The extent of the agreement reflects whether the biosynthetic and dehydrogenase fluxes comprising the solution set are accurate.

Solution Method

With the present formulation, a system of 16 equations and unknowns can be solved. Alternately, "best fit" flux values for fluxes can be obtained by using more of the available information, which includes errors acknowledged. The alternative entails adding a consistency Eq. (5a) to the equation set, thereby generating 16 unknown fluxes and 17 equations. However, the quality of the data and overall solution are still reflected by the degree of the consistency equations satisfied.

The 16×17 problem can be solved by the least-squares method as follows [18, 19]: If **b**, **A**, and **c** denote the column vector of the unknown fluxes (16×1), coefficient matrix of the flux equations (17×16), and constant vector of the flux equations (17×1), respectively, the flux equations can be represented by

$$\mathbf{Ab=c} \quad (2a)$$

The error in each balance can be included by rewriting Eq. (2a) as

$$\mathbf{Ab+e=c} \quad (2b)$$

where **e** is the error vector (17×1). The sum of the squares of the errors, Σ, is

$$\Sigma=(\mathbf{c}-\mathbf{Ab})^T(\mathbf{c}-\mathbf{Ab}) \quad (2c)$$

and minimizing Σ with respect to each flux gives the best value of **b** as follows:

$$\mathbf{A}^T\mathbf{Ab}=\mathbf{A}^T\mathbf{c} \quad (2d)$$

The "best-fit" solution can be readily obtained using packages such as GAMS 2.20 (General Algebraic Modeling System, VAX VMS version).

ATP Yield

Dividing the cell mass formation rate by the ATP generation rate provides the ATP yield coefficient (g cell/mol ATP). The ATP generation rate is obtained by summing all the ATP forming fluxes. If it is assumed that the P/O ratio is 2 and 1 for the turnover of NADH and $FADH_2$, respectively, the generation rate is

ATP generation rate
=(generation from glycolysis and TCA cycle)
+(generation from NADH and $FADH_2$)
$=(-r_{12}+r_{14}+r_{18}+r_{23}+r_{27})+(2r_{14}+2r_{21}+2r_{27}+2r_{29}$
-2(lactate flux)$+r_{29}$). (3)

The ATP yield coefficient is thus given by 1000D divided by the ATP generation rate obtained from Eq. (3), where D denotes the dilution rate.

Table 1A. Metabolic fluxes for *E. coli* B/r cultivated in 1 g/l glucose medium.

Flux*	D=0.20 h^{-1}	D=0.48 h^{-1}	D=0.75 h^{-1}
r_1	2.76	6.55	12.3
r_2	0.245	1.41	3.86
r_3	0.0400	0.0990	0.155
r_4	0.217	0.821	1.86
r_5	0.042	0.578	1.88
r_6	0.175	0.433	0.676
r_7	0.056	0.375	1.06
r_8	0	0.190	0.691
r_9	0.0704	0.174	0.272
r_{10}	2.48	5.02	8.11
r_{11}	0.0138	0.0342	0.0535
r_{12}	2.54	5.54	9.66
r_{13}	0.0252	0.0623	0.0973
r_{14}	5.06	11.2	19.8
r_{15}	0.291	0.720	1.12
r_{16}	4.77	10.5	18.6
r_{17}	0.140	0.347	0.542
r_{18}	1.41	2.13	3.13
r_{19}	0	0	0
r_{20}	0.552	1.37	2.13
r_{21}	3.62	7.31	13.2
r_{22}	0.571	1.42	2.21
r_{23}	0	0	4.93
r_{24}	3.04	5.89	6.00
r_{25}	3.05	5.87	5.86
r_{26}	0.211	0.522	0.814
r_{27}	2.87	5.34	4.92
r_{28}	0	0	0
r_{29}	2.89	5.33	4.82
r_{30}	0.349	0.865	1.35
r_{31}	0.476	1.44	2.63
r_{32}	9.62	19.2	26.3

* Flux units are mmol/g cell /h.

RESULTS

Flux Patterns for Chemostat Cultivated *E. coli* B/r

The metabolic fluxes determined for the chemostat-cultivated *E. coli* B/r are summarized in Table 1A. For growth in a 1 g/l glucose medium, the organic acid production was limited to acetate (2.0 mM at 0.75 h^{-1}), which appeared between a 0.48 and 0.75 h^{-1} dilution rate [5].

The results of the consistency tests are shown in Table 1B. The carbon and CO_2 balances were extremely close for the low growth rates. The worst discrepancies occur with red for the O_2 balances, which were attributed to calculating the O_2 consumption by subtracting two comparable partial pressures. Overall, the balances were reasonably close.

Based on the fluxes presented in Table 1A, certain trends were identified. For example, the ATP production by aerobic glycolysis (substrate level including acetate formation plus NADH turnover, i.e. $-r_{12}+r_{14}+r_{18}+r_{23}+2r_{14}+2r_{21}$) constituted approximately 50% of the total ATP at the lowest growth rate examined (0.20 h^{-1}). The contribution increased to 80% at the highest growth rates. Other significant flux trends are summarized in Fig. 2A. The glucose consumption rate increased linearly with the growth rate. However, the acetate production exhibited a higher growth

Table 1B. Consistency tests of *E. coli* B/r fluxes for cultivation in 1 g/l medium.

	D=0.20 h^{-1}	D=0.48 h^{-1}	D=0.75 h^{-1}
Measured CO_2 evolution	9.62	19.2	26.3
Calculated CO_2 evolution[1]	9.61	19.2	26.4
Input carbon	16.6	39.3	73.8
Output carbon[2]	16.9	37.3	64.4
Measured O_2 consumption	7.30	18.8	24.9
Calculated O_2 consumption[3]	9.01	18.1	25.1

Flux units are mmol/g cell/h.

[1]Calculated CO_2 evolution rate$=r_2+r_{21}+r_{25}+r_{27}-r_{31}+1.52$ D, where the constant term, 1.52, is for the byproduct from the biosynthesis.

[2]Carbon output rate$=(\beta r_{19}+2r_{23}+4r_{28}+r_{32})+0.45$ D 1000/12, where the constant term, 0.45, is the carbon fraction of the cell mass, and 12 is the molecular weight of carbon.

[3]Calculated O_2 evolution rate$=(3.578$ D$+r_{14}+r_{21}+r_{27}+2r_{29})/2$, where the constant term, 3.578, is for the formation of NADH from the biosynthesis as a byproduct.

rate threshold for growth on a 1 g/l glucose medium. Moreover, as the growth rate increased, the TCA cycle fluxes increased, and then attained the maxima or declined. In contrast to the TCA cycle flux trends, the fraction of the TCA cycle flux used for biosynthesis increased as the growth rate increased.

Yield for Chemostat-Cultivated *E. coli* B/r

Figure 2B summarizes the respiratory quotient (RQ), fraction of carbon converted to CO_2, cell yield coefficient, and ATP yield coefficient. The RQ was approximately unity and depended weakly on the growth rate, in agreement with other reports [21]. The decline indicates that the cell's respiratory metabolism diminished at a higher dilution rate. The percentage of glucose converted to CO_2 decreased rapidly with an increasing growth rate. This decrease was consistent with the increased secretion of organic acids at higher growth rates. The cell yield ranged between 0.3–0.4 g cell/g glucose and depended on the dilution rate and glucose concentration, which is typical for this strain [21]. The ATP yield coefficients were found to range from 4 to

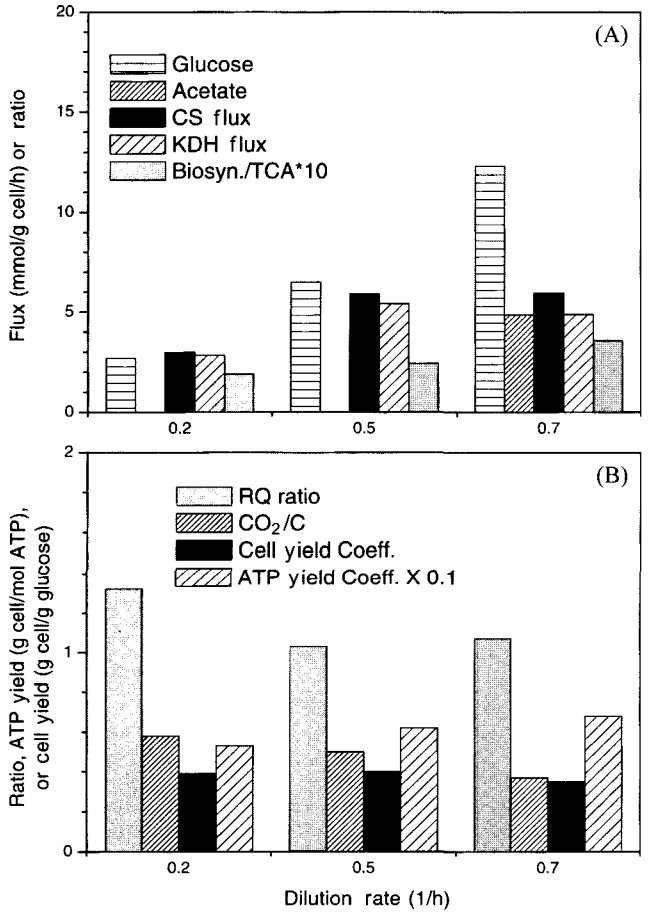

Fig. 2. (A) Flux trends for *E. coli* B cultivated in chemostat on 1 g/l glucose medium. (B) Respiratory quotient and yield trends for *E. coli* B cultivated in chemostat on 1 g/l glucose medium.

Table 2A. Metabolic fluxes for *E. coli* K12 cultivated in 1 g/l glucose medium.

Flux*	D=0.2 h^{-1}	D=0.6 h^{-1}
r_1	4.22	12.9
r_2	0.252	4.39
r_3	0.041	0.123
r_4	0.223	1.92
r_5	0.047	2.38
r_6	0.179	0.538
r_7	0.061	1.29
r_8	0.003	1.01
r_9	0.0722	0.217
r_{10}	3.95	8.27
r_{11}	0.0142	0.0425
r_{12}	4.02	10.4
r_{13}	0.0258	0.0774
r_{14}	8.03	21.7
r_{15}	0.299	0.896
r_{16}	7.74	20.8
r_{17}	0.144	0.431
r_{18}	3.00	5.36
r_{19}	0	0
r_{20}	0.567	1.70
r_{21}	6.66	16.5
r_{22}	0.586	1.76
r_{23}	2.90	12.6
r_{24}	3.16	2.13
r_{25}	3.18	2.03
r_{26}	0.216	0.647
r_{27}	3.04	1.30
r_{28}	0	0
r_{29}	3.08	1.23
r_{30}	0.357	1.07
r_{31}	0.395	2.05
r_{32}	13.1	23.0

* Flux units are mmol/g cell/h.

6 g cell/mol ATP. Although these values were lower than the theoretical value (29 g cell/mole ATP [25]), they compared well with the other reported values [7]. Overall, the flux and yield trends indicated that as the growth rate increased, ATP was produced increasingly by aerobic glycolysis, carbon was spilled as acetate and other organic acids, and the role of TCA cycle became more biosynthetic.

Flux and Yield Patterns for Chemostat Cultivated *E. coli* K12 (JM101)

The fluxes associated with the chemostat cultivation of *E. coli* K12 at two dilution rates are shown in Table 2A. The results of the consistency tests are shown in Table 2B; closure to within 10% was attained. Some key flux and yield patterns are shown in Figs. 3A and 3B, respectively. For growth in a 1 g/l glucose medium, the growth rate dependence of the fluxes and yields was qualitatively similar to that of the B/r strain. Namely, an increasing growth rate resulted in acetate production, reduced the

Table 2B. Consistency tests of *E. coli* K12 fluxes for cultivation in 1 g/l glucose medium.

	D=0.2 h^{-1}	D=0.6 h^{-1}
Measured CO_2 evolution	13.1	23.0
Calculated CO_2 evolution[1]	13.0	23.1
Input carbon	25.3	77.4
Output carbon[2]	26.4	70.7
Measured O_2 evolution	8.95	26.2
Calculated O_2 evolution[3]	12.3	22.1

*Flux units are mmol/g cell/h.

[1]Calculated CO_2 evolution rate=$r_2+r_{21}+r_{25}+r_{27}-r_{31}+1.52$ D, where the constant term, 1.52, is for the byproduct from the biosynthesis.

[2]Carbon output rate=$(\beta r_{19}+2r_{23}+4r_{28}+r_{32})+0.45$ D 1000/12, where the constant term, 0.45, is the carbon fraction of the cell mass, and 12 is the molecular weight of carbon.

[3]Calculated O_2 evolution rate=$(3.578\ D+r_{14}+r_{21}+r_{27}+2r_{29})/2$, where the constant term, 3.578, is for the formation of NADH from the biosynthesis as a byproduct.

TCA cycle fluxes, and devoted more TCA cycle flux to biosynthesis. Moreover, the proportion of ATP produced by aerobic glycolysis increased with the growth rate (68 to 90%). The K12 strain differed from the B/r strain by being considerably more glycolytic, as reflected by a higher acetate production and lower yield on glucose.

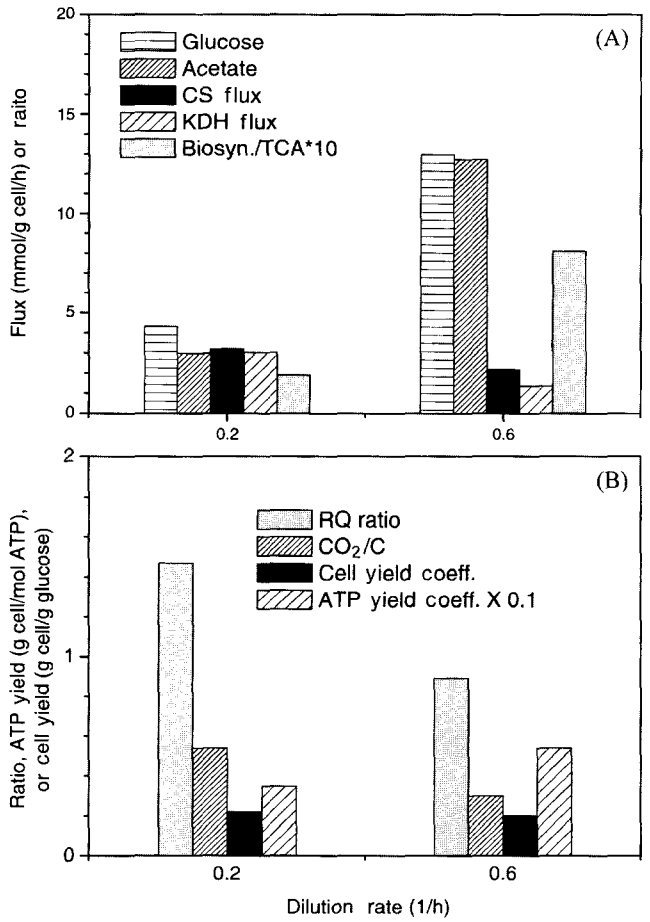

Fig. 3. (A) Flux trends for *E. coli* K12 cultivated in chemostat on 1 g/l glucose medium. (B) Respiratory quotient and yield trends for *E. coli* K12 cultivated in chemostat on 1 g/l glucose medium.

Testing Analysis Approach on Citrate Synthase Deficient Mutant

The modeling approach was tested by determining if a mutant's metabolism could be predicted. Accordingly, a mutant deficient in citrate synthase was investigated. Since the enzyme deficiency can be overcome by providing proline in addition to glucose, if the stoichiometric assumptions made in developing the flux analysis method are valid and general, then it should be possible to predict the range of proline-glucose ratios that will support the growth of the mutant.

The citrate synthase deficiency was represented by deleting r_{24} from the metabolic map (Fig. 1), thus partially isolating the TCA cycle from the glycolytic pathway. When proline is used as a second carbon source, two extreme versions of metabolism are possible, as shown in Fig. 4. In Scheme A, glycolysis provides oxaloacetate for the biosynthetic requirements, thus minimizing the use of proline as a carbon skeleton. Most of the nitrogen required

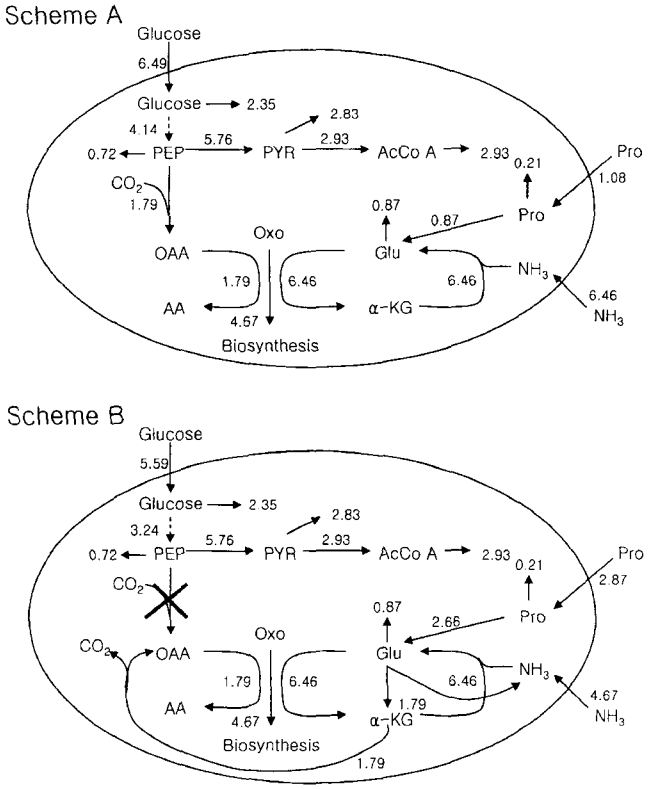

Fig. 4. Possible metabolic schemes for citrate synthase deficient mutant using proline and glucose as carbon sources. Scheme A depicts the extreme where glucose provides all the carbon for oxaloacetate synthesis.

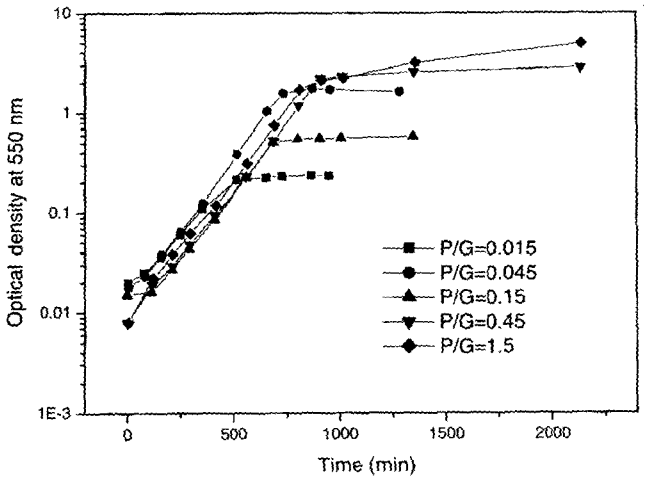

Fig. 5. Batch growth of mutant deficient in citrate synthase when the proline-glucose ratio (P/G) is varied. The initial glucose concentration was fixed at 1 g/l in all experiments.

for amino acid synthesis is not provided by proline, but from inorganic ammonia. Scheme B differs in that all the carbon extracted from the TCA cycle for biosynthesis is provided by proline. In this case, the TCA cycle is completely separated from the glycolysis. Moreover, the minimum amount of ammonia is used in the amination biosynthetic reactions.

In practice, the mutant's metabolism will likely fall between the extremes of Schemes A and B. Based on the flux analysis method, the predicted molar ratio of proline to glucose ranged from 0.17 to 0.50. When comparing Scheme A to B, Scheme A also predicted a lower production of CO_2 and higher consumption of NH_3.

The results of the batch growth experiments where the initial proline concentration was varied are shown in Fig. 5. Only for the proline-to-glucose ratios (P/G) of 0.015 and 0.045 was residual glucose detected in the growth medium in the stationary state, indicating that for these ratios, proline was limiting. For the other ratios, the culture attained similar densities following logarithmic growth, which were either sustained (P/G=0.15) or increased slowly afterward (P/G= 0.45 and 1.5). Since the mutant exhibited a slow growth on a medium containing only proline as a carbon source (data not shown.), the slow secondary growth phase was due to the metabolism of the residual proline. Thus, the experiments indicated that the stoichiometry of proline-to-glucose lay between 0.15 and 0.45, which compared well with the predicted value.

DISCUSSION

The fluxes were compared with previously reported enzyme activity trends to see if any correlations existed between induction-repression behavior and flux. The existence of a correlation for a particular enzyme would suggest that the enzyme may exercise significant flux control. Considering first the glycolytic enzymes, prior chemostat studies performed with a feed glucose concentration comparable to that used in this study (1 g/l) indicated that phosphofructokinase, fructose diphosphate aldolase, lactate dehydrogenase, and pyruvate kinase activities increase only slightly and attain weak maxima or asymptotic values as the growth rate increases [8]. The results for both *E. coli* B/r and K12 revealed that the phosphofructokinase, fructose diphosphate aldolase, lactate dehydrogenase, and pyruvate kinase fluxes all increased in proportion to the growth rate. Consequently, this relationship suggests that these enzyme activities do not constrain flux.

In contrast to the aforementioned glycolytic enzymes, the pyruvate kinase flux in both strains increased the least in response to an increased growth rate. Moreover, examining the PEP (phosphoenol pyruvate) branch point more closely revealed that as the growth rate increased, the ratio of phosphoenolpyruvate carboxylase to the pyruvate kinase flux increased proportionally with the growth rate. This increasing ratio indicates that pyruvate kinase became increasingly less able to compete for the common metabolite, PEP, as the growth rate increased. Such diminished competition indicates that a branch point control mechanism was operating, whereby as the cellular biosynthetic activity increased, more glucose carbon was directed to oxaloacetate formation than oxidation via the TCA cycle. For example, pyruvate kinase is more easily saturated than phosphoenolpyruvate carboxylase; hence, as the glucose flux, and in turn, triose formation increased, the saturated pyruvate kinase branch resulted in the phosphoenolpyruvate carboxylase branch taking up the slack. The higher affinity of pyruvate kinase for PEP compared to phosphoenolpyruvate carboxylase (30 vs. 630 μM [23, 29]) is consistent with this scenario.

Regarding TCA cycle enzymes, α-ketoglutarate dehydrogenase, succinate dehydrogenase, and malate dehydrogenase activities have been previously reported to decrease, or attain a maxima, and thereafter significantly decline with an increasing growth rate [4, 8, 30]. In addition, these enzymes have been reported to be repressed in a batch culture during exponential growth on glucose [1, 6]. α-Ketoglutarate dehydrogenase appears to be particularly volatile where, for example, activity is barely detectable in a batch culture [1] and significant repression occurs in chemostat cultures at a high growth rate [4].

The TCA fluxes determined in the current study showed such enzyme activity patterns. For *E. coli* K12, increasing the dilution rate from 0.2 to 0.6 h^{-1} was accompanied by decreased citrate synthase and α-ketoglutarate dehydrogenase fluxes, where the latter decreased the most (60% reduction; see Table 2A and Fig. 3B). *E. coli* B/r exhibited a similar, yet less dramatic decrease in the citrate synthase and α-ketoglutarate dehydrogenase fluxes as the growth rate

increased. Taken together, declining TCA cycle enzyme activities mapped with decreasing *in vivo* fluxes suggest that the TCA cycle may present flux bottlenecks for rapidly growing cells.

While it is widely recognized that rapidly growing cells exhibit "aerobic fermentation" due to diminished oxidative metabolism or depressed Krebs cycle activity, the current results shed some light on the mechanistic details. In addition, the predictions of the acetate overflow analysis are supported. The greater reduction in the α-ketoglutarate dehydrogenase activity and *in vivo* flux compared to the citrate synthase activity and flux suggests that α-ketoglutarate dehydrogenase is highly flux controlling as opposed to the TCA cycle's "gateway enzyme," citrate synthase. Moreover, due to this flux control, the loss of Krebs cycle activity can be mostly attributed to the repression of α-ketoglutarate dehydrogenase activity. The high capacity of glycolysis coupled with a TCA bottleneck located at α-ketoglutarate dehydrogenase then results in acetate overflow at high growth rates. This conclusion agrees with an earlier analysis that determined incomplete glucose oxidation, as reflected by the onset of acetate secretion, is likely due to a limiting TCA enzymatic activity as opposed to constrained NADH turnover at the level of the cytochrome chain [15].

Apart from possibly explaining why acetate overflow occurs, a flux constraint at α-ketoglutarate dehydrogenase is reasonable from the biosynthetic point of view. This enzyme is located at the branch point where the biosynthetic enzyme, glutamate dehydrogenase, converts the common metabolite α-ketoglutarate to glutamate. If *in vitro* enzymological results are translatable to *in vitro* conditions, glutamate dehydrogenase's lower affinity for α-ketoglutarate confers a competitive disadvantage for the common metabolite [14]. However, repressing α-ketoglutarate dehydrogenase has the effect of equalizing the disadvantage, thereby improving the ability to transform α-ketoglutarate to glutamate. This branch point control system is economical in that more biosynthetic flux is acquired for a fixed, or even decreasing, input flux provided by the entry enzyme, citrate synthase.

Although differing in some mechanistic features, this control strategy has also been observed in another TCA branch point that participates in acetate metabolism. Isocitrate dehydrogenase and isocitrate lyase compete for the TCA metabolite, isocitrate. Based on *in vitro* studies, the former's affinity exceeds the latter's. However, instead of repression, phosphorylation decreases isocitrate dehydrogenase activity, thereby increasing the isocitrate flux, which in turn allows acetate to be metabolized via the glyoxylate bypass [26, 27].

It is interesting that a branch point mechanism involving the alteration of a high-affinity enzyme's activity is responsible for both acetate formation and consumption. However, the dynamics of branch point control enabling consumption are considerably more rapid than those for production. It can be speculated that *E. coli* acquires a competitive advantage by being able to expend ATP to rapidly adjust to changes in carbon source availability. Under circumstances of an abundant energy source, slower mechanisms are used to fine-tune this metabolism, which can waste carbon. Although such wastage may appear to be inefficient, the ability to store carbon in the medium represents a form of efficiency, as previously discussed by Holms. Moreover, the ability to rapidly utilize the carbon store adds to the efficiency and competitiveness of the regulatory strategy.

To infer what metabolic fluxes are associated with a particular growth rate and carbon/energy source, mass balance approaches were used in conjunction with reported data and experimental measurements. This work represents a demonstration of the utility of attaining fluxes and provides a useful starting point for developing alternative balance approaches that more fully utilize experimental data that can be attained with high accuracy. As a related approach, a flow network modeling method was used to predict the behavior of a citrate synthase-deficient mutant.

NOMENCLATURE

Symbols

AcCOA, acetyl coenzyme A; CIT, citrate; E4P, erythrose-4-phosphate; F6P, fructose-6-phosphate; G6P, glucose-6-phosphate; KG, α-ketoglutarate; OAA, oxaloacetate; PEP, phosphoenol pyruvate; 3PG, 3-phosphoglycerate; PYR, pyruvate; R5P, ribose-5-phosphate; Ribulose 5P, ribulose-5-phosphate; Succ, succinate; TP, triose phosphate; and Xylulose 5P, xylulose-5-phosphate

Notation

A : Coefficient matrix (17×16)
C_i's : Concentration of organic acid, mmol/l
D : Dilution rate, h^{-1}
S_0, S : Input and output glucose concentration, respectively, mmol/l
X : Biomass concentration, g cell/l
b : Column vector of unknown fluxes (16×1)
c : Constant vector of flux equations (17×1)
e : Error vector (17×1)
r : Flux, mmol/g cell/h
β: Moles of carbon per mole of organic acid
Σ: Sum of squares of the errors

Acknowledgment

The present research was conducted partly based on a Research Grant from Kwangwoon University in 2001.

REFERENCES

1. Amarasingham, C. R. and B. D. Davis. 1965. Regulation of α-ketoglutarate dehydrogenase formation in *Escherichia coli*. *J. Biol. Chem.* **240:** 3664–3668.
2. Beitle, R. R. and M. M. Ataai. 1991. A unique cultivation monitoring and control system. *Biotechnology Techniques* **5:** 77–82.
3. Dawes, I. W. and J. Mandelstam. 1970. Sporulation of *Bacillus subtilis* in continuous culture. *J. Bacteriol.* **103:** 529–535.
4. Doelle, H. W., K. N. Ewingw, and N. W. Hollywood. 1982. Regulation of glucose metabolism in bacterial systems. *Advances in Biochemical Engineering* **23:** 1–35.
5. El-Mansi, E. M. T. and W. H. Holms. 1989. Control of carbon flux to acetate excretion during growth of *Escherichia coli* in batch and continuous cultures. *Journal of General Microbiology* **135:** 2875–2883.
6. Gray, C. T., J. W. T. Wimpenny, and M. R. Mossman. 1966. Regulation of metabolism in facultative bacteria. II. Effects of aerobiosis, anaerobiosis and nutrition on the formation of Krebs cycle enzymes in *Escherichia coli*. *Biochim. Biophys. Acta* **117:** 33–41.
7. Hempfling, W. P. and S. E. Mainzer. 1975. Effects of varying the carbon source limiting growth on yield and maintenance characteristics of *Escherichia coli* in continuous culture. *J. Bacteriol.* **123:** 1076–1087.
8. Hollywood, N. and H. W. Doelle. 1976. Effect of specific growth rate and glucose concentration on growth and glucose metabolism of *Escherichia coli* K-12. *Microbios.* **17:** 23–33.
9. Holms, W. H. 1986. The central metabolic pathway of *Escherichia coli*: Relationship between flux and control at a branch point, efficiency of conversion to biomass, and excretion of acetate. *Curr. Top. Cell. Reg.* **28:** 69–105.
10. Ingraham, J. L., O. Maaloe, and F. C. Neidhardt. 1983. *Growth of the Bacterial Cell.* Sinauer Associates, Inc., Sunderland, Massachusetts.
11. Kacser, H. and J. A. Burns. 1973. The control of flux. *Symp. Soc. Exp. Biol.* **27:** 65–104.
12. Lakshmi, T. M. and R. B. Helling. 1976. Selection for citrate synthase deficiency in icd mutants of *Escherichia coli*. *J. Bacteriol.* **127:** 76–83.
13. Lee, J., A. Goel, M. M. Ataai, and M. M. Domach. 1994. Flux adaptations of citrate synthase-deficient *Escherichia coli*. *Ann. Acad. Sci.* **745:** 35–50.
14. Majewski, R. A. and M. M. Domach. 1990. Effect of regulatory mechanism on hyperbolic reaction network properties. *Biotechnol. Bioeng.* **36:** 166–178.
15. Majewski, R. A. and M. M. Domach. 1990. Simple constrained-optimization view of acetate overflow in *E. coli*. *Biotechnol. Bioeng.* **35:** 732–738.
16. Mandelstam, J., K. McQuillen, and I. Dawes. 1982. *Biochemistry of Bacterial Growth.* 3rd ed., Halsted Press, New York - Toronto.
17. Niranjan, S. C. and K.-Y. San. 1989. Analysis of a framework using material balances in metabolic pathways to elucidate cellular metabolism. *Biotechnol. Bioeng.* **34:** 496–500.
18. Noble, B. 1969. *Applied Linear Algebra.* Prentice-Hall, Inc. pp. 39–46.
19. Papoutsakis, E. T. and C. L. Meyer. 1985. Equations and calculations of product yields and preferred pathways for butanediol and mixed-acid fermentations. *Biotechnol. Bioeng.* **27:** 50–66.
20. Postma, P. W. 1987. Phosphotransferase system for glucose and other sugars. *In* F. C. Neidhardt, J. L. Ingraham, K. B. Low, B. Magasanik, M. Schaechter, and H. E. Umbarger (eds.), *Escherichia coli and Salmonella typhimurium - Cellular and Molecular Biology*, American Society for Microbiology. pp. 127–141.
21. Reiling, H. E., H. Laurila, and A. Fiechter. 1985. Mass culture of *Escherichia coli*: Medium development for low and high density cultivation of *Escherichia coli* B/r in minimal and complex media. *J. Biotech.* **2:** 191–206.
22. Reissig, J. L. and E. L. Wollman, 1963. Transduction des marqueurs galactose par les bacteriophages temperes 82 et 434 d'*Escherichia coli*. *Ann. Inst. Pasteur.* **105:** 774–779.
23. Smith, T. E. 1968. *Escherichia coli* phosphoenolpyruvate carboxylase: Characterization and sedimentation behavior. *Arch. Biochem. Biophys.* **128:** 611–622.
24. Spencer, M. E. and J. R. Guest. 1982. Molecular cloning of four tricarboxylic acid cycle genes of *Escherichia coli*. *J. Bacteriol.* **151:** 542–552.
25. Stouthamer, A. H. 1979. The search for correlation between theoretical and experimental growth yields. *In* J. R. Quayle (ed.), *Microbial Biochemistry*, University Park Press, Baltimore.
26. Walsh, K. and D. E. Koshland, Jr. 1985. Branch point control by the phosphorylation state of isocitrate dehydrogenase: A quantitative examinaton of fluxes during a regulatory transition. *J. Biol. Chem.* **260:** 8430–8437.
27. Walsh, K. and D. E. Koshland, Jr. 1984. Determination of flux through the branch point of two metabolic cycles: The tricarboxylic acid cycle and the glyoxylate shunt. *J. Biol. Chem.* **259:** 9646–9654.
28. Wang, N. S. and G. Stephanopoulos. 1983. Application of macroscopic balances to the identification of gross measurement errors. *Biotechnol. Bioeng.* **25:** 2177–2208.
29. Waywood, E. B. and B. D. Sanwal. 1974. The control of pyruvate kinase of *Escherichia coli*. *J. Biol. Chem.* **249:** 265–280.
30. Weitzman, P. D. J. 1982. Unity and diversity in some bacterial citric acid-cycle enzymes. *Advances in Microbial Physiology* **22:** 185–244.
31. Wong, H. H., R. V. Van Wegen, J. Choi, S. Y. Lee, and A. P. J. Middelberg. 1999. Metabolic analysis of poly(3-hydroxybutyrate) production by recombinant *Escherichia coli*. *Journal of Microbiology and Biotechnology* **9:** 593–603.
32. Yanisch-Perron, C., J. Vieira, and J. Messing. 1985. Improved M13 phage cloning vectors and host strains: Nucleotide sequences of the M13mp18 and pUC19 vectors. *Gene* **33:** 103–119.

APPENDIX : Formulation of Metabolic Pathways

Formulating the material balances is simplified by invoking the pseudo-steady-state assumption, which is valid because metabolite concentrations are typically much smaller than the magnitude of metabolite fluxes [19]. The 16 mass balances are as follows:

$$r_1=r_2+r_3+r_{10} \quad \text{(A1a)}$$
$$r_{10}=r_{11}+r_{12}-r_7-r_8 \quad \text{(A1b)}$$
$$2r_{12}=r_{13}+r_{14}-r_8 \quad \text{(A1c)}$$
$$r_{14}=r_{15}+r_{16} \quad \text{(A1d)}$$
$$r_{16}=r_1+r_{17}+r_{18}+r_{31} \quad \text{(A1e)}$$
$$r_{18}=r_{19}+r_{20}+r_{21}-r_1 \quad \text{(A1f)}$$
$$r_{24}=r_{29}+r_{31}-r_{30} \quad \text{(A1g)}$$
$$r_{21}=r_{22}+r_{23}+r_{24} \quad \text{(A1h)}$$
$$r_{24}=r_{25} \quad \text{(A1i)}$$
$$r_{25}=r_{26}+r_{27} \quad \text{(A1j)}$$
$$r_{27}=r_{28}+r_{29} \quad \text{(A1k)}$$
$$r_2=r_4+r_5 \quad \text{(A1l)}$$
$$r_4=r_6+r_7 \quad \text{(A1m)}$$
$$r_5=r_7+r_8 \quad \text{(A1n)}$$
$$r_7=r_8+r_9 \quad \text{(A1o)}$$
$$r_{32}=r_2+r_{21}+r_{25}+r_{27}-r_{31}+1.52D \quad \text{(A1p)}$$

where D denotes the dilution rate and the constant term of Eq. (A1p), 1.52 mmol/g cell, is for the byproduct from biosynthesis.

The measurable fluxes can be determined from analyses of the cell culture supernatants. The glucose consumption rate (r_1) can be calculated from the difference between the input (S_0) and output (S) glucose concentration

$$r_1=(S_0-S)\,D/X \quad \text{(A2)}$$

where X represents the biomass concentration (g cell/l). The organic acid byproducts fluxes (r_{19}, r_{23}, and r_{28}) can be determined from concentration measurements in a similar manner

$$r_{19}=C_{organics}\,D/X \quad \text{(A3a)}$$
$$r_{23}=C_{acetate}\,D/X \quad \text{(A3b)}$$
$$r_{28}=C_{succinate}\,D/X \quad \text{(A3c)}$$

The net rate of NADPH production from glucose oxidation in the pentose phosphate pathway and isocitrate dehydration is estimated to be equal to the biosynthetic requirement of 18 mmol NADPH/g cell [10]. Thus, the NADPH production rate is

$$2r_2+r_{25}=18\,D \quad \text{(A4)}$$

where 2 moles of NADPH are assumed to be synthesized per mole of glucose converted to ribulose-5-phosphate.

How the values of 11 biosynthetic fluxes are computed from the data in the reference [13] can be illustrated by formulating r_{20}. Assume for this example that the dilution rate is 0.48 h^{-1}. The flux, r_{20}, represents the consumption rate of pyruvate for the production of amino acids and peptidoglycan. By adding the numbers in the pyruvate (PYR) column, which corresponds to the conversion of pyruvate to amino acids, and multiplying by the dilution rate, the value of r_{20} can be obtained; namely, r_{20}=(0.488+0.276+0.856+0.326+0.804+0.0276+0.0552 mmol/g cell) * (0.48 h^{-1})=(1.36 mmol/g cell /h).